

Surface electronic state of superconducting topological crystalline insulator

Tatsuki Hashimoto, Keiji Yada, and Yukio Tanaka

Department of Applied Physics, Nagoya University, Nagoya 464-8603, Japan

Masatoshi Sato

Yukawa Institute for Theoretical Physics, Kyoto University, Kyoto 604-8317, Japan

(Dated: June 12, 2019)

We study surface state of a doped topological crystalline insulator in the superconducting state. Motivated by $\text{Sn}_{1-x}\text{In}_x\text{Te}$, we consider fully-gapped pair potentials and calculate the surface spectral function. It is found that mirror-protected zero-energy Andreev bound states appear at the (001) surface and that these states can move along the mirror symmetric line on the surface Brillouin zone. We also show that the surface Andreev bound state changes systematically with doping due to the presence of the Dirac surface state in the normal state.

I. INTRODUCTION

The existence of the surface Andreev bound state (SABS) is an important physical property of unconventional superconductivity [1–3]. SABSs appear on the surface (edge) of a three (two) dimensional unconventional superconductor with a pair potential that changes its sign on the Fermi surface [1, 4–7] and have been detected experimentally in cuprate [1, 7] and Sr_2RuO_4 [8, 9] by tunneling spectroscopy. The topological origin of SABS has been clarified based on the topological invariants defined in the bulk Hamiltonian. Because of bulk-boundary correspondence, superconductors with gapless SABSs are now called topological superconductors [10, 11], and the concept of topological superconductivity has been expanding widely [12–22].

On the other hand, topological insulators, topological crystalline insulators (TCIs), Weyl semimetals and Dirac semimetals have been of great interest because these materials exhibit novel surface states [23–28]. It has now been shown that these topological materials can be superconducting state at low temperatures. It has been also predicted that these superconducting states can host previously unobserved exotic SABSs if the surface states in the normal state remain gapless even in the superconducting state. Superconducting topological insulator (STI), Cu doped Bi_2Se_3 , is a notable examples of such a material. Following the observation of zero-bias conductance peak that indicates the existence of SABS [29], determination of the pairing symmetry of $\text{Cu}_x\text{Bi}_2\text{Se}_3$ is recognized as an important problem and $\text{Cu}_x\text{Bi}_2\text{Se}_3$ has become a subject of intense research interest [30–45]. If odd-parity pairing is realized, SABS in this material can have a twisted dispersion called “Caldela cone” due to the mixing with the surface state in the normal state [46–48]. Superconducting Dirac semimetals are another remarkable example of novel superconductors. Most recently, superconductivity in Dirac semimetal Cd_3As_2 has been found experimentally [49–51] and the existence of exotic surface state has been predicted theoretically [52]. Superconductivity has been also studied theoretically in the Weyl semimetal and quantum anomalous Hall sys-

tem [53–57]. Notably, crossed SABSs originating from the Fermi arc are expected to appear in Weyl semimetal superconductors [54].

For TCIs, superconductivity has been reported in In doped SnTe [58]. In point contact measurements, $\text{Sn}_{1-x}\text{In}_x\text{Te}$ shows zero-bias conductance peak that may originate from SABS [59]. Thus, this material is expected to be a topological superconductor. In the normal state, SnTe has mirror-protected double Dirac cones along the mirror symmetric line on (001) surface [26, 60, 61]. Therefore, it is likely that, similar to the other superconducting topological materials, superconducting TCIs (STCIs) exhibit a new type of SABS. Using the similarity of low energy electronic state to $\text{Cu}_x\text{Bi}_2\text{Se}_3$, Sasaki *et. al.* have investigated the superconducting state of $\text{Sn}_{1-x}\text{In}_x\text{Te}$ with an effective model for around each L point (See Fig.1) [59]. However, different from $\text{Cu}_x\text{Bi}_2\text{Se}_3$ which has a single Fermi surface, $\text{Sn}_{1-x}\text{In}_x\text{Te}$ has four hole pockets around the L points and two hole pockets are projected to the same position in the surface Brillouin zone for the (001) surface. To reveal the surface state including the effect of the overlap of the Fermi surfaces, it is necessary to consider the entire Brillouin zone.

In this paper, we study the SnTe class TCI in the superconducting state using a tight-binding model which can represent the electronic states for the entire Brillouin zone. We introduce possible fully-gapped pair potentials for the TCI and calculate the surface spectral function using the recursive Green’s function method. It is found that the STCI can host mirror-protected SABSs. Furthermore, the SABSs exhibit twisted dispersion due to merging with the surface Dirac cone in the normal state. In contrast to STIs, we find that in STCI, the position of zero-energy SABS in the surface Brillouin zone can move along the mirror symmetric line with changes in the material parameters. Therefore, the dispersion of the SABSs in STCI does not necessarily become flat at zero energy due to twisting. To understand the topological nature of this material in more detail, we also calculate the mirror Chern number and construct the phase diagram in terms of the magnitudes of the pairing potential and the spin-orbit interaction. We find that phases with the mirror Chern numbers $n_M = 0, -2, -4$ is present in

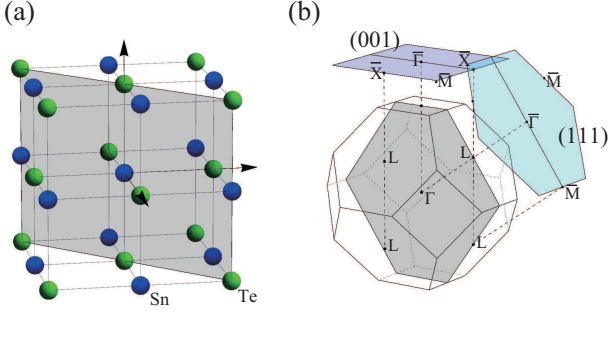


FIG. 1. (a) Crystal structure of SnTe. (b) First Brillouin zone of a rock salt crystal and, (001) and (111) surface Brillouin zone. The shaded planes are (110) mirror invariant planes.

STCI. This feature is different from the three phases in STIs with mirror Chern numbers $n_M = 0, -1, -2$.

This paper is organized as follows. In Sec.II, we review a tight-binding model proposed by Lent *et. al.* for IV-VI semiconductors and propose possible pair potentials for the tight-binding model. We also show the calculation method of the spectral function. The topological nature of the TCI with possible pair potentials is discussed in Sec.III. In Sec.IV, we show the calculated results of spectral function for the (001) surface and discuss the evolution of the mirror-protected SABS. In Sec.V, we discuss the experimental situation and the surface state for a time-reversal breaking pairing. Finally, we summarize our results in Sec.VI.

II. MODEL AND FOMULATION

A. Model for SnTe and $\text{Sn}_{1-x}\text{In}_x\text{Te}$

We briefly review the topological crystalline insulator SnTe [26]. In Fig.1, we show the crystal structure, the first Brillouin zone and the surface Brillouin zone of SnTe. The crystal of SnTe has the face centered cubic structure, which belongs to O_h point group. The band inversion occurs at four L points. For the cubic structure, the (001) surface is particularly unique because two L points are projected to the same \bar{X} points on the surface Brillouin zones. In this case, two surface Dirac cones show up at the same \bar{X} points with different energies. The Dirac cones mix with each other and thus have gap in general. However, on $\bar{\Gamma}-\bar{X}$ mirror symmetric line, the Dirac cones remain gapless because each Dirac cone belongs to different mirror subspace. These surface states have been observed by angle resolved photoemission spectroscopy (ARPES) experiments [60, 61]. It is noted that even if In is doped, SnTe still has the gapless Dirac cones [62].

To describe the normal state of the TCI, we use a tight-binding model proposed by C. S. Lent *et. al.* [63]. This

model Hamiltonian is a 36×36 matrix with nine orbitals, i.e. s , p^3 , d^5 , two spin degrees of freedom and two sublattices (anion and cation). The Hamiltonian has the following nearest neighbor hopping and the on-site spin-orbit interaction, which is given by

$$\hat{H}_{\text{SnTe}} = \begin{pmatrix} \hat{H}_{s,s} & \hat{H}_{pc,s}^\dagger & \hat{H}_{pa,s}^\dagger & 0 & 0 \\ \hat{H}_{pc,s} & \hat{H}_{pc,pc} & \hat{H}_{pa,pc}^\dagger & 0 & \hat{H}_{da,pc}^\dagger \\ \hat{H}_{pa,s} & \hat{H}_{pa,pc} & \hat{H}_{pa,pa} & \hat{H}_{dc,pa}^\dagger & 0 \\ 0 & 0 & \hat{H}_{dc,pa} & \hat{H}_{dc,dc} & \hat{H}_{da,dc}^\dagger \\ 0 & \hat{H}_{da,pc} & 0 & \hat{H}_{da,dc} & \hat{H}_{da,da} \end{pmatrix}. \quad (1)$$

Here, indices a and c denote anion and cation, respectively, and we take the basis as follows, $(c_{s,c,\uparrow}, c_{s,c,\downarrow}, c_{s,a,\uparrow}, c_{s,a,\downarrow}, c_{p_x,c,\uparrow}, c_{p_x,c,\downarrow}, c_{p_z,c,\uparrow}, c_{p_z,c,\downarrow}, c_{p_y,c,\uparrow}, c_{p_y,c,\downarrow}, c_{p_z,c,\downarrow}, c_{p_y,a,\uparrow}, c_{p_y,a,\downarrow}, c_{p_z,a,\uparrow}, c_{p_z,a,\downarrow}, c_{d_1,c,\uparrow}, c_{d_2,c,\uparrow}, c_{d_3,c,\uparrow}, c_{d_4,c,\uparrow}, c_{d_5,c,\uparrow}, c_{d_1,c,\downarrow}, c_{d_2,c,\downarrow}, c_{d_3,c,\downarrow}, c_{d_4,c,\downarrow}, c_{d_5,c,\downarrow}, c_{d_1,a,\uparrow}, c_{d_2,a,\uparrow}, c_{d_3,a,\uparrow}, c_{d_4,a,\uparrow}, c_{d_5,a,\uparrow}, c_{d_1,a,\downarrow}, c_{d_2,a,\downarrow}, c_{d_3,a,\downarrow}, c_{d_4,a,\downarrow}, c_{d_5,a,\downarrow})$. See the original paper for the explicit form of the Hamiltonian and the parameters for SnTe [63]. The BdG Hamiltonian for the superconducting state is given by

$$\hat{H}_{\text{BdG}} = [\hat{H}_{\text{SnTe}} - \mu \hat{I}] \hat{\tau}_z + \hat{\Delta}_i \hat{\tau}_x, \quad (2)$$

where $\hat{\tau}_i$ represents the Pauli matrix in the Nambu space, μ is the chemical potential, \hat{I} is an identity matrix and $\hat{\Delta}_i$ is the pair potential. The basis is taken to be $(c_{\alpha,\beta,\uparrow}, c_{\alpha,\beta,\downarrow}, -c_{\alpha,\beta,\downarrow}^\dagger, c_{\alpha,\beta,\uparrow}^\dagger)$, with $\alpha = s, p_x, p_y, p_z, d_1, d_2, d_3, d_4, d_5$ and $\beta = a, c$.

Up to now, almost all experiments for superconducting state in $\text{Sn}_{1-x}\text{In}_x\text{Te}$, e.g. specific heat[64–66], μ -SR measurements[67] and thermal conductivity[68], have suggested the fully-gapped superconductivity. One of the candidates of the fully-gapped superconducting state is s -wave pair potential, which is a spin-singlet even-parity on-site pair potential. Hereafter, we denote this pair potential as Δ_1 . For p -wave pair potential in the cubic lattice, there are four types of time-reversal-invariant pairing, A_{1u} , E_u , T_{1u} and T_{2u} , as summarized in Refs.[69–72]. The energy gap of A_{1u} pairing is fully gapped. While the other pairings give point or line nodes. Thus, according to the experimental results, we focus on A_{1u} pair potential, and hereafter, we denote the A_{1u} pair potential as Δ_2 . Δ_2 is a spin-triplet odd-parity one, which is similar to that for the BW phase of ^3He . Δ_2 is composed of two electrons on the nearest neighbor sites, i.e., Sn and Te sites. Below, we assume that Cooper pairs are formed within the p orbitals and ignore the s and d orbitals since low energy band is mainly composed of p orbitals. For simplicity, we also assume that electrons in p_i orbital ($i = x, y, z$) form Cooper pair along i -direction. The explicit form of the pair potentials are given by

$$\hat{\Delta}_1 = \Delta \sum_{i=x,y,z} \hat{p}_i \hat{s}_0 \hat{\sigma}_0, \quad (3)$$

$$\hat{\Delta}_2 = \Delta \sum_{i=x,y,z} \sin \frac{k_i}{2} \hat{p}_i \hat{s}_i \hat{\sigma}_x, \quad (4)$$

Pair potential	O_h	spin	I	$M_{(110)}$	energy gap
Δ_1		A_{1g}	singlet	+	full gap
Δ_2		A_{1u}	triplet	-	full gap

TABLE I. Possible pair potentials for the STCI. Δ_1 (Δ_2) is even (odd) under inversion operation. Δ_1 (Δ_2) is even (odd) under the (110) mirror reflection operation.

where \hat{s}_i and $\hat{\sigma}_i$ are the Pauli matrices of the spin and sublattice, respectively. In this basis, \hat{s}_0 (\hat{s}_μ ($\mu = x, y, z$)) denotes the spin singlet (spin triplet) and σ_0 (σ_x) denotes the intra(inter)-site pairing. \hat{p}_i is the following matrix

$$\hat{p}_i = \begin{pmatrix} 0 & 0 & 0 & 0 & 0 & 0 & 0 & 0 & 0 & 0 \\ 0 & \delta_{ix} & 0 & 0 & 0 & 0 & 0 & 0 & 0 & 0 \\ 0 & 0 & \delta_{iy} & 0 & 0 & 0 & 0 & 0 & 0 & 0 \\ 0 & 0 & 0 & \delta_{iz} & 0 & 0 & 0 & 0 & 0 & 0 \\ 0 & 0 & 0 & 0 & 0 & 0 & 0 & 0 & 0 & 0 \\ 0 & 0 & 0 & 0 & 0 & 0 & 0 & 0 & 0 & 0 \\ 0 & 0 & 0 & 0 & 0 & 0 & 0 & 0 & 0 & 0 \\ 0 & 0 & 0 & 0 & 0 & 0 & 0 & 0 & 0 & 0 \\ 0 & 0 & 0 & 0 & 0 & 0 & 0 & 0 & 0 & 0 \\ 0 & 0 & 0 & 0 & 0 & 0 & 0 & 0 & 0 & 0 \end{pmatrix}, \quad (5)$$

in the basis, $(c_{s,\beta,\gamma}, c_{p_x,\beta,\gamma}, c_{p_y,\beta,\gamma}, c_{p_z,\beta,\gamma}, c_{d_1,\beta,\gamma}, c_{d_2,\beta,\gamma}, c_{d_3,\beta,\gamma}, c_{d_4,\beta,\gamma}, c_{d_5,\beta,\gamma})$, where $\beta = a, c$ and $\gamma = \uparrow, \downarrow$. The pair potentials also have the mirror reflection symmetry with respect to the (110) plane. Δ_1 (Δ_2) is even (odd) under the mirror reflection

$$\mathcal{M}_{(110)} \hat{\Delta}_1 \mathcal{M}_{(110)}^\dagger = \hat{\Delta}_1, \quad (6)$$

$$\mathcal{M}_{(110)} \hat{\Delta}_2 \mathcal{M}_{(110)}^\dagger = -\hat{\Delta}_2, \quad (7)$$

where $\mathcal{M}_{(110)}$ is the (110) mirror operator. Since Δ_1 has an even-parity under the (110) mirror operation, H_{BdG} commutes with

$$\mathcal{M}_{(110)}^+ = \begin{pmatrix} \mathcal{M}_{(110)} & 0 \\ 0 & \mathcal{M}_{(110)}^* \end{pmatrix}, \quad (8)$$

in the mirror invariant plane. On the other hand, Δ_2 has an odd parity under the (110) mirror operation. Therefore, H_{BdG} can be block diagonalized under the diagonal basis of a mirror operator

$$\mathcal{M}_{(110)}^- = \begin{pmatrix} \mathcal{M}_{(110)} & 0 \\ 0 & -\mathcal{M}_{(110)}^* \end{pmatrix}, \quad (9)$$

We summarize the characters of the pair potentials in Table I.

B. Recursive Green's function method

To calculate the SABS in the STCI, we use recursive Green's function method. Here, we briefly review the

method using Möbius transformation in the semi-finite system proposed by Umerski [73].

First, to express the (001) surface, we transform the k_z component of the BdG Hamiltonian into real space. Then, we define the matrix

$$\hat{X} = \begin{pmatrix} 0 & \hat{t}^{-1} \\ -\hat{t}^\dagger & (\xi \hat{1} - \hat{h}) \hat{t}^{-1} \end{pmatrix}, \quad (10)$$

where \hat{t} and \hat{h} are 72×72 matrices describing $+z$ component and k_x - k_y plane component of the BdG Hamiltonian, respectively. Thus, \hat{X} is a 144×144 matrix. z is a complex number and $\hat{1}$ is an identity matrix. Next, we diagonalize the matrix \hat{X} by a matrix \hat{O}

$$\hat{O}^{-1} \hat{X} \hat{O} = \begin{pmatrix} \lambda_1 & & & 0 \\ & \lambda_2 & & \\ & & \ddots & \\ 0 & & & \lambda_{144} \end{pmatrix}, \quad (11)$$

with $|\lambda_1| > |\lambda_2| > \dots > |\lambda_{144}|$. Then, we define four square matrices in \hat{O}_{ij} with $i, j = 1, 2$ as follows,

$$\hat{O} = \begin{pmatrix} \hat{O}_{11} & \hat{O}_{12} \\ \hat{O}_{21} & \hat{O}_{22} \end{pmatrix}. \quad (12)$$

Finally, we obtain the surface Green's function,

$$\hat{G} = \hat{O}_{12} [\hat{O}_{22}]^{-1}. \quad (13)$$

For the retarded Green's function, we put $\xi = \omega + i\delta$ where ω and δ denote the frequency and an infinitesimal number, respectively. By using \hat{G} , the surface spectral function is given by,

$$A(\omega, k_x, k_y) = -\frac{1}{\pi} \text{Im}[\text{Tr}(\hat{G})]. \quad (14)$$

III. TOPOLOGICAL NATURE

In this section, we clarify topological nature of the STCI, based on the recently expanded topological periodic table that includes crystalline symmetries in addition to time-reversal and particle-hole symmetries [74–76]. First of all, we briefly review topological nature of normal state, the TCI. In terms of Altland-Zirnbauer (AZ) classification [77–80], the TCI belongs to class AII, since it has the time-reversal symmetry for fermions. However, the corresponding Z_2 topological number is trivial, because band inversion occurs at an even number (four) of time-reversal invariant momenta. Thus, the time-reversal symmetry is not sufficient to explain the surface states in the TCI. Instead, the mirror reflection symmetry, which is specific to the crystal structure of the TCI, is responsible for the stability of the surface states in the TCI. Taking into account the mirror reflection symmetry, SnTe is classified as class AII with U_+^-

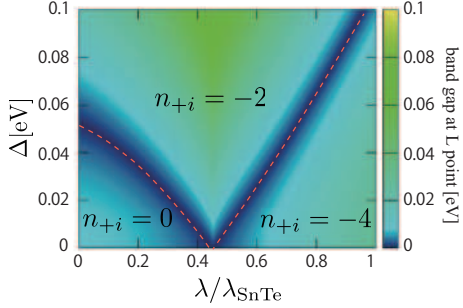


FIG. 2. Phase diagram of superconducting topological crystalline insulator with the odd-parity full-gapped pair potential Δ_2 as a function of the magnitude of the pair potential Δ and spin-orbit interaction $\lambda/\lambda_{\text{SnTe}}$. Color shows the magnitude of the energy gap at L point. Red dotted lines show gap closed line.

with $d = 3$ and $d_{\parallel} = 1$ in Ref. [75], because the mirror operator $\mathcal{M}_{(110)}$ commutes with time-reversal operator \mathcal{T} and obeys $\mathcal{M}_{(110)}^2 = -1$. Therefore, its topological nature is characterized by the mirror Chern number

$$n_M = \frac{n_{+i} - n_{-i}}{2}. \quad (15)$$

Here, $n_{\pm i}$ is the Chern number for mirror subsectors labeled with mirror eigenvalues $\pm i$. It has been known that the mirror Chern number for the TCI is -2 [26].

In terms of the AZ classification, the STCI with Δ_2 belongs to class DIII. The superconducting state also possesses the mirror reflection symmetry. The mirror operator $\mathcal{M}_{(110)}^-$ obeys $(\mathcal{M}_{(110)}^-)^2 = -1$ and commutes (anticomutes) with time reversal operator \mathcal{T} (chiral operator \mathcal{C}). Thus, this system belongs to class DIII with U_{+-}^- with $d = 3$ and $d_{\parallel} = 1$. In this case topological nature is characterized with two integer numbers, $Z \oplus Z$. One of the integer numbers is three-dimensional winding number. Though the exact calculation of the winding number is difficult because of the huge Hamiltonian matrix, its parity can be easily obtained by using Fermi surface criteria [81]. In the present case, the Fermi surfaces enclose four time reversal invariant momenta, i.e. L points. Thus, the winding number must be an even number. The other topological number is the mirror Chern number which can be defined on a two-dimensional mirror plane in the Brillouin. We calculate the mirror Chern number as a function of the magnitude of the spin-orbit interaction and the pair potential using the method proposed by Suzuki *et. al* [82]. In Fig.2, we show the topological phase diagram of the STCI with Δ_2 . The color shows the band gap at the L point. Here, we set $\mu = 0.27$ eV. The mirror Chern number changes $-4 \rightarrow -2 \rightarrow 0$ with gap closing. This is different from the case in the STI, since the mirror Chern number of the STI changes $-2 \rightarrow -1 \rightarrow 0$ [47].

For Δ_2 , the BdG Hamiltonian on the mirror invariant plane can be divided into two eigenvectors of the mirror

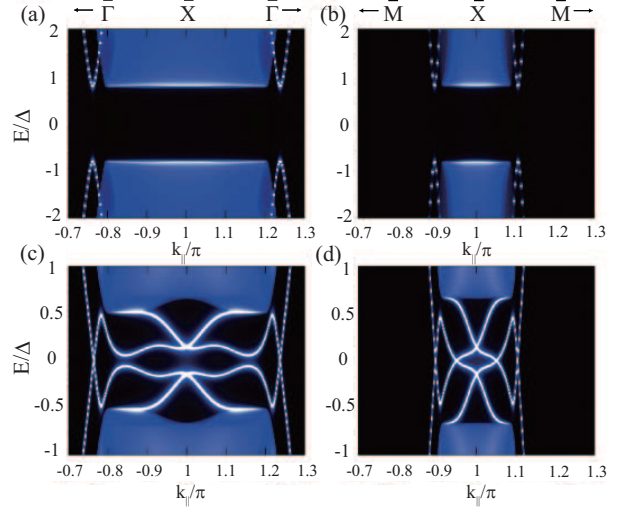


FIG. 3. Surface spectral function for the (001) surface. (a) and (b) show the spectral function for the even-parity spin-singlet pair potential Δ_1 along mirror symmetric $\bar{\Gamma}-\bar{X}-\bar{\Gamma}$ line and $\bar{M}-\bar{X}-\bar{M}$ line, respectively. (c) and (d) show the spectral function for the odd-parity spin-triplet pair potential Δ_2 along mirror symmetric $\bar{\Gamma}-\bar{X}-\bar{\Gamma}$ line and $\bar{M}-\bar{X}-\bar{M}$ line, respectively. In the case of Δ_1 , there is no Andreev bound state in the superconducting gap. On the other hand, there are mirror-protected zero-energy Andreev bound state.

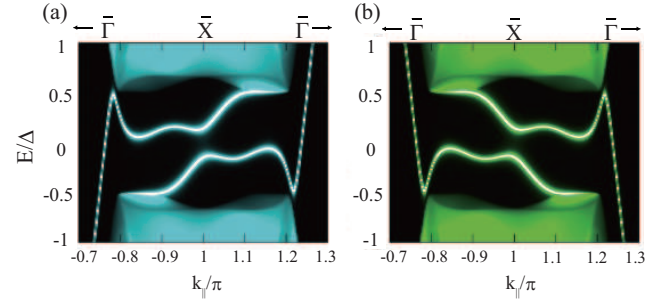


FIG. 4. Mirror separated spectral function in the case of Δ_2 for (a)+i and (b)-i along the mirror symmetric line $\bar{\Gamma}-\bar{X}-\bar{\Gamma}$.

operator in Eq.9, each of which belongs to class *D*. This state is the topological crystalline superconducting state defined in Ref. [83] since each subsector has particle-hole symmetry.

IV. SURFACE SPECTRAL FUNCTION

In this section, we present our numerically calculated results of the surface spectral function for the (001) surface. In this calculation, we set $\Delta = 0.06$ eV in Eqs. (3) and (4). The chemical potential is taken as $\mu = -0.2$ eV to fit the size of Fermi surface observed in ARPES measurements [62]. In this case, the conduction band and the

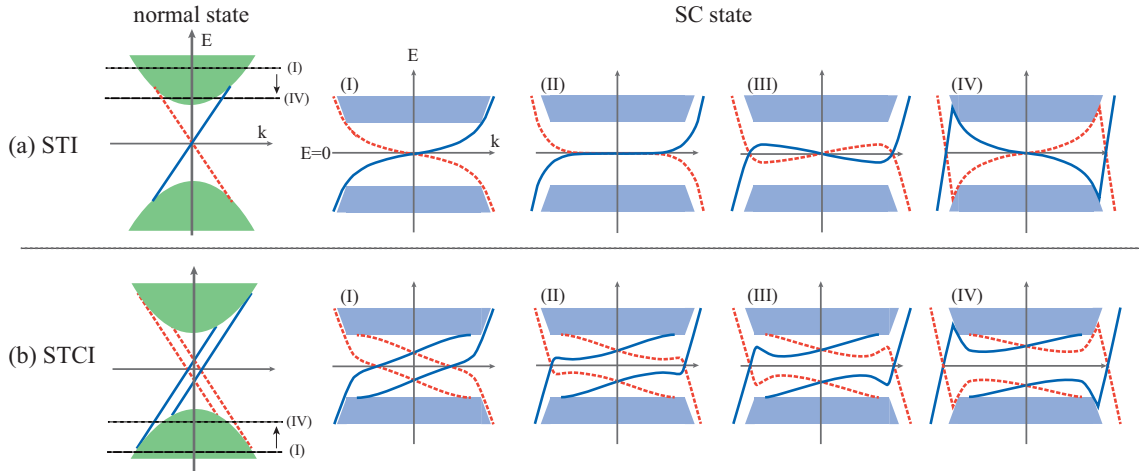


FIG. 5. Systematic change of the surface Andreev bound state (SABS) in the superconducting topological insulator (STI) (a) and the superconducting topological crystalline insulator (STCI) (b). Blue solid (red dotted) lines show the SABS for the mirror $+i(-i)$ sector. The SABS changes depending on the position of the chemical potential. Here, we assume $\text{Cu}_x\text{Bi}_2\text{Se}_3$ and $\text{Sn}_{1-x}\text{In}_x\text{Te}$ for STI and STCI, respectively. For this reason, the figure of normal state for the STI (STCI) is depicted as the electron (hole) doped case. In both cases, carrier number decreases from the panel (I) to (IV).

TCI surface state are well separated at the Fermi level, and the mirror Chern number is -2 . First, we show the surface spectral function for Δ_1 . Figures. 3 (a) and (b) show the spectral function along the $\bar{\Gamma}-\bar{X}-\bar{\Gamma}$ and $\bar{M}-\bar{X}-\bar{M}$ lines, respectively. In the case of Δ_1 , both bulk and TCI surface states have a superconducting gap and there is no inner gap state. As is seen from Figs.3 (a) and (b), the magnitude of the gap minima is $E/\Delta = 0.8$ instead of $E/\Delta = 1$ for a single band model with s -wave pair potential, since we introduce the pair potential only for p -orbitals. In Figs. 3 (c) and (d), we show the surface spectral function for Δ_2 . Figure. 3 (c) shows the surface spectral function along the $\bar{\Gamma}-\bar{X}-\bar{\Gamma}$ line, i.e. mirror symmetric line. As is seen from the figure, there are two zero-energy SABSs corresponding to the mirror Chern number $= -2$. Different from the Dirac cone in the TCI, the surface state in the superconducting state is twisted since the SABSs merge into the TCI Dirac cone. Using the mirror reflection operator, we decompose the surface spectral function into two subsectors with different eigenvalue $\pm i$ as shown in Fig. 4. As we mentioned in Sec. III, the Chern number of each subsector $\pm i$ is ∓ 2 . Therefore, there are two chiral SABSs in each subsector. There are also zero-energy SABSs along $\bar{M}-\bar{X}-\bar{M}$ line (See Fig. 3(d)). These zero energy SABSs can be interpreted by zero-dimensional topological number defined by combining with $\mathcal{M}_{(110)}$ and \mathcal{C} [52]. These zero-energy SABSs disappear if we enlarge the magnitude of Δ like $\Delta = 0.1$ eV.

We now turn to the detail analysis on the mirror protected SABS which appears in the case of Δ_2 . First, we briefly review the systematic change of the SABS in the STI such as $\text{Cu}_x\text{Bi}_2\text{Se}_3$ [46–48]. In the case of the STI, the structure of the SABS changes mainly with the chem-

ical potential. If the Fermi level is much higher than the energy where surface state is merged into bulk band, the shape of the SABS is like a cone, which is similar to that of the ^3He BW phase, as can be seen in Fig.5 (a) (I). On the other hand, as lower the Fermi level, the SABS starts twisting as shown in Fig.5 (a) (III) and, finally, the SABS become like Fig.5 (a) (IV). Furthermore, it has been revealed that between the non-twisting and twisting cases, the dispersion becomes flat like as shown in Fig.5 (a) (II) since the position of zero energy SABS is pinned at time reversal invariant momenta, i. e. $k = 0$. This flat-like band can explain the ZBCP in the point-contact experiments even if the bulk energy spectrum is fully gapped [46–48].

Next, we reveal the structural transition of the SABS in the STCI. If the Fermi level is much lower than the energy where the TCI surface state is merged into the bulk band, there are two Dirac cones on the mirror plane as shown in Fig.5 (b) (I). On the other hand, in the same manner as the STI, if the chemical potential is located on the energy where surface and bulk states are well separated, the dispersion of the SABS in the STCI is twisted as shown in Fig.5(b)(IV). However, different from the SABS in the STI, that in the STCI does not have to host flat-like dispersion at zero energy between the twisting (I) and non-twisting (IV) cases as shown in Fig.5.(b) (II) and (III). Different from the case of STI, the zero-energy SABS in the STCI is not protected by the time reversal symmetry but the mirror symmetry. Therefore, the position of the zero-energy SABS in the surface Brillouin zone can move along the mirror symmetric line. For this reason, the mirror protected SABS in the STCI can twist without presenting the flat-like band at zero energy.

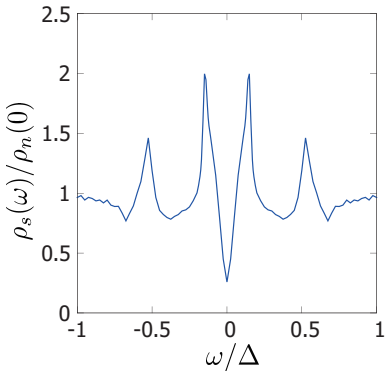


FIG. 6. Surface density of state in the case of Δ_2 for the (001) surface with $\Delta = 0.02$ eV. There are four peaks at $\omega/\Delta = \pm 0.49$ and ± 0.16

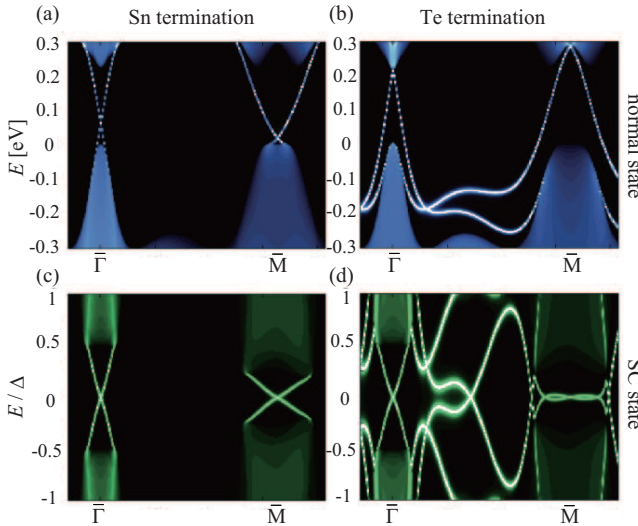


FIG. 7. Surface spectral function for the (111) surface along mirror symmetric line $\bar{\Gamma}-\bar{M}$. (a) and (b) show the surface spectral function of the normal state for Sn and Te terminated surface, respectively. (c) and (d) show the spectral function of superconducting state for Sn and Te terminated surface, respectively. Here, we set the chemical potential $\mu = -0.2$ eV, which is the same as the calculation for the (001) surface.

V. INTERPRETATION OF EXPERIMENTS AND DISCUSSION

We discuss the experimental situation for the tunneling spectroscopy. First, we show our numerically calculated results of normalized surface density of state $\rho_s(\omega)/\rho_n(0)$ in the case of Δ_2 for the (001) surface as a function of energy ω . Here, we set $\Delta = 0.02$ eV. As can be seen from Fig.6, there are four peaks at $\omega/\Delta = \pm 0.49$ and ± 0.16 . Therefore, it is reasonable that four peaks appear in con-

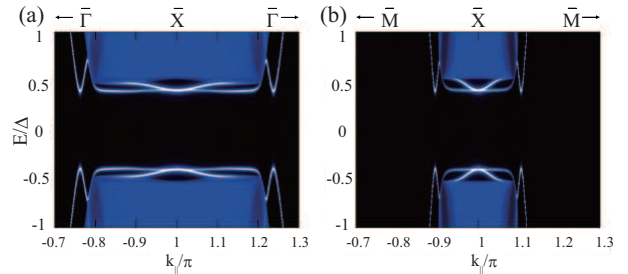


FIG. 8. Surface spectral function in the case of $\Delta_2 + i\Delta_1$ pairing. We introduce Δ_1 and Δ_2 at the same ratio.

ductance measurement with low transmissivity realized in scanning tunneling spectroscopy (STS). On the other hand, in the point-contact measurements, it is likely to include the components of the surface with different orientations since the surface of crystal contains many steps in the contact region.

Since the point-contact spectra may contain the tunneling other than the (001) surface, we calculate the surface spectral function for the (111) surface as an example of different surfaces. In the case of the (111) surface, L points are projected to either $\bar{\Gamma}$ point or \bar{M} points as shown in Fig 1 (b). Moreover, there are two distinct situations, i.e. Sn-terminated surface and Te-terminated surface. In Fig. 7 (a)((b)), the spectral function for Sn(Te)-terminated surface in the normal state is presented. In the case of the Sn-terminated surface, Dirac points are located on the high symmetric points $\bar{\Gamma}$ and \bar{M} . On the other hand, in the case of Te-terminated surface, Dirac points appear on the mirror symmetric line $\bar{\Gamma}-\bar{M}$. In Fig.7 (c)((d)), we show the Sn(Te)-terminated surface spectral function in the superconducting state for Δ_2 . As can be seen from the figures, the SABSs for the (111) surface is completely different from those for the (001) surface. In the case of Sn-terminated surface, two cone-shape surface states appear at the $\bar{\Gamma}$ and \bar{M} points on the surface Brillouin zone corresponding to mirror Chern number $n_M = -2$. In this case, the structural change of the SABS is almost the same as that of the STI. In the case of Te-terminated surface, as you can see in Fig.7 (d), the surface state at \bar{M} point is flat like and there are zero-energy surface states between the $\bar{\Gamma}$ and \bar{M} points since the valley surface state remains due to the existence of the mirror reflection symmetry.

From the above calculation, it is reasonable to conclude that the bias voltage dependence of conductance for the (001) surface can be changed from the four peaks spectra if the component of the (111) surface is included. In addition, in the normal state, it has been revealed that the edge state of (001) film dramatically changes depending on the number of layers [84]. It can be expected that the similar changes of the ABS may occur in the superconducting state because of the existence of the steps on the surface. Therefore, further calculations is necessary

to interpret the obtained point-contact experiments [59].

Before closing this section, we briefly refer to the case of $\Delta_2 + i\Delta_1$ i.e. $p + is$ pairing which breaks time-reversal symmetry. Novak *et. al.* have indicated the realization of $p + is$ pairing in $\text{Sn}_{1-x}\text{In}_x\text{Te}$ by point-contact experiments [64]. Theoretically, P. Goswami and B. Roy have suggested the possibility of the $p + is$ pairing in doped topological materials with an effective model [85]. Motivated by the studies, we calculate the spectral function for $\Delta_2 + i\Delta_1$ state in the lattice model. The calculated results are shown in Fig.8. Consequently, we find that even in the lattice model, the system has gapped SABS since $\Delta_2 + i\Delta_1$ pairing breaks the (110) mirror symmetry. Our model is useful for further discussion of anomalous thermal Hall effect in $\text{Sn}_{1-x}\text{In}_x\text{Te}$.

VI. CONCLUSION

In this paper, we have theoretically studied the SnTe class TCI in the superconducting state. We have introduced the possible fully-gapped pair potentials to the TCI and calculated the surface spectral function using the recursive Green's function method. We have found that the STCI hosts the mirror-protected SABSs whose

dispersion has never been seen before. It has been revealed that SABSs are twisted in the energy dispersion since they merge into the surface Dirac cone stemming from the normal state. We have shown that the zero-energy SABSs can move along the mirror symmetric line on the surface Brillouin zone. It is clarified that the dispersion of the SABSs for the (001) surface is not necessary to become flat at zero energy when it twists. We also find that four peaks appear in the SDOS, which can be detected by STS measurements.

VII. ACKNOWLEDGEMENTS

We thank A. Yamakage, S. Kobayashi and H. Ozawa for valuable discussions. This work was supported by the “Topological Quantum Phenomena” Grant-in-Aid for Scientific Research on Innovative Areas from the Ministry of Education, Culture, Sports, Science and Technology (MEXT) of Japan (No. 22103005), the “Topological Materials Science” Grant-in-Aid for Scientific Research on Innovative Areas from the MEXT of Japan (No. 15H05853, 15H05855), Grant-in-aid for JSPS Fellows (No. 26010542) (TH) and Grant-in-Aid for Scientific Research B (No. 25287085) (MS).

[1] S. Kashiwaya and Y. Tanaka, *Rep. Prog. Phys.* **63**, 1641 (2000).

[2] T. Löfwander, V. S. Shumeiko, and G. Wendin, *Supercond. Sci. Technol.* **14**, R53 (2001).

[3] G. Deutscher, *Rev. Mod. Phys.* **77**, 109 (2005).

[4] L. J. Buchholtz and G. Zwicknagl, *Phys. Rev. B* **23**, 5788 (1981).

[5] J. Hara and K. Nagai, *Prog. Theor. Phys.* **76**, 1237 (1986).

[6] C. R. Hu, *Phys. Rev. Lett.* **72**, 1526 (1994).

[7] Y. Tanaka and S. Kashiwaya, *Phys. Rev. Lett.* **74**, 3451 (1995).

[8] M. Yamashiro, Y. Tanaka, and S. Kashiwaya, *Phys. Rev. B* **56**, 7847 (1997).

[9] S. Kashiwaya, H. Kashiwaya, H. Kambara, T. Furuta, H. Yaguchi, Y. Tanaka, and Y. Maeno, *Phys. Rev. Lett.* **107**, 077003 (2011).

[10] Y. Tanaka, M. Sato, and N. Nagaosa, *J. Phys. Soc. Jpn.* **81**, 011013 (2012).

[11] J. Alicea, *Rep. Prog. Phys.* **75**, 076501 (2012).

[12] C. L. M. Wong, J. Liu, K. T. Law, and P. A. Lee, *Phys. Rev. B* **88**, 060504 (2013).

[13] P. M. R. Brydon, A. P. Schnyder, and C. Timm, *Phys. Rev. B* **84**, 020501 (2011).

[14] A. P. Schnyder and S. Ryu, *Phys. Rev. B* **84**, 060504 (2011).

[15] A. P. Schnyder and P. M. R. Brydon, *J. Phys.: Condens. Matter* **27**, 243201 (2015).

[16] M. Sato, Y. Tanaka, K. Yada, and T. Yokoyama, *Phys. Rev. B* **83**, 224511 (2011).

[17] Y. Tanaka, Y. Mizuno, T. Yokoyama, K. Yada, and M. Sato, *Phys. Rev. Lett.* **105**, 097002 (2010).

[18] K. Yada, M. Sato, Y. Tanaka, and T. Yokoyama, *Phys. Rev. B* **83**, 064505 (2011).

[19] M. Sato, Y. Takahashi, and S. Fujimoto, *Phys. Rev. Lett.* **103**, 020401 (2009).

[20] R. M. Lutchyn, J. D. Sau, and S. Das Sarma, *Phys. Rev. Lett.* **105**, 077001 (2010).

[21] Y. Oreg, G. Refael, and F. von Oppen, *Phys. Rev. Lett.* **105**, 177002 (2010).

[22] J. Alicea, *Phys. Rev. B* **81**, 125318 (2010).

[23] Y. Ando, *Journal of the Physical Society of Japan* **82**, 102001 (2013).

[24] M. Z. Hasan and C. L. Kane, *Rev. Mod. Phys.* **82**, 3045 (2010).

[25] X.-L. Qi and S.-C. Zhang, *Rev. Mod. Phys.* **83**, 1057 (2011).

[26] T. H. Hsieh, H. Lin, J. Liu, W. Duan, A. Bansil, and L. Fu, *Nature Communications* **3** (2012).

[27] X. Wan, A. M. Turner, A. Vishwanath, and S. Y. Savrasov, *Phys. Rev. B* **83**, 205101 (2011).

[28] B.-J. Yang and N. T. Nagaosa, *Nature Communications* **5**, 4898 (2014).

[29] S. Sasaki, M. Kriener, K. Segawa, K. Yada, Y. Tanaka, M. Sato, and Y. Ando, *Phys. Rev. Lett.* **107**, 217001 (2011).

[30] Y. S. Hor, A. J. Williams, J. G. Checkelsky, P. Roushan, J. Seo, Q. Xu, H. W. Zandbergen, A. Yazdani, N. P. Ong, and R. J. Cava, *Phys. Rev. Lett.* **104**, 057001 (2010).

[31] S. Sasaki and T. Mizushima, *Physica C: Superconductivity and its Applications* **514**, 206 (2015), *superconducting Materials: Conventional, Unconventional and Undetermined*.

[32] T. Hashimoto, K. Yada, A. Yamakage, M. Sato, and Y. Tanaka, *Superconductor Science and Technology* **27**,

104002 (2014).

[33] T. Hashimoto, K. Yada, A. Yamakage, M. Sato, and Y. Tanaka, *Journal of the Physical Society of Japan* **82**, 044704 (2013).

[34] S. Takami, K. Yada, A. Yamakage, M. Sato, and Y. Tanaka, *Journal of the Physical Society of Japan* **83**, 064705 (2014).

[35] Y. Nagai, H. Nakamura, and M. Machida, *Phys. Rev. B* **86**, 094507 (2012).

[36] Y. Nagai, H. Nakamura, and M. Machida, *Journal of the Physical Society of Japan* **84**, 033703 (2015).

[37] Y. Nagai, *Journal of the Physical Society of Japan* **83**, 063705 (2014).

[38] Y. Nagai, H. Nakamura, and M. Machida, *Journal of the Physical Society of Japan* **83**, 064703 (2014).

[39] S.-K. Yip, *Phys. Rev. B* **87**, 104505 (2013).

[40] L. Fu and E. Berg, *Phys. Rev. Lett.* **105**, 097001 (2010).

[41] L. Fu, *Phys. Rev. B* **90**, 100509 (2014).

[42] M. Kriener, K. Segawa, Z. Ren, S. Sasaki, and Y. Ando, *Phys. Rev. Lett.* **106**, 127004 (2011).

[43] M. Kriener, K. Segawa, S. Sasaki, and Y. Ando, *Phys. Rev. B* **86**, 180505 (2012).

[44] T. V. Bay, T. Naka, Y. K. Huang, H. Luigjes, M. S. Golden, and A. de Visser, *Phys. Rev. Lett.* **108**, 057001 (2012).

[45] B. Zocher and B. Rosenow, *Phys. Rev. B* **87**, 155138 (2013).

[46] A. Yamakage, K. Yada, M. Sato, and Y. Tanaka, *Phys. Rev. B* **85**, 180509 (2012).

[47] T. H. Hsieh and L. Fu, *Phys. Rev. Lett.* **108**, 107005 (2012).

[48] L. Hao and T. K. Lee, *Phys. Rev. B* **83**, 134516 (2011).

[49] L. Aggarwal, A. Gaurav, G. S. Thakur, Z. Haque, A. K. Ganguli, and G. Sheet, *ArXiv e-prints* (2014), arXiv:1410.2072 [cond-mat.supr-con].

[50] H. Wang, H. Wang, H. Liu, H. Lu, W. Yang, S. Jia, X.-J. Liu, X. C. Xie, J. Wei, and J. Wang, *ArXiv e-prints* (2015), arXiv:1501.00418 [cond-mat.supr-con].

[51] L. P. He, Y. T. Jia, S. J. Zhang, X. C. Hong, C. Q. Jin, and S. Y. Li, *ArXiv e-prints* (2015), arXiv:1502.02509 [cond-mat.supr-con].

[52] S. Kobayashi and M. Sato, *ArXiv e-prints* (2015), arXiv:1504.07408 [cond-mat.supr-con].

[53] G. Y. Cho, J. H. Bardarson, Y.-M. Lu, and J. E. Moore, *Phys. Rev. B* **86**, 214514 (2012).

[54] B. Lu, K. Yada, M. Sato, and Y. Tanaka, *Phys. Rev. Lett.* **114**, 096804 (2015).

[55] A. Ii, A. Yamakage, K. Yada, M. Sato, and Y. Tanaka, *Phys. Rev. B* **86**, 174512 (2012).

[56] A. Ii, K. Yada, M. Sato, and Y. Tanaka, *Phys. Rev. B* **83**, 224524 (2011).

[57] X.-L. Qi, T. L. Hughes, and S.-C. Zhang, *Phys. Rev. B* **82**, 184516 (2010).

[58] G. S. Bushmarina, I. A. Drabkin, V. Kompaniets, R. Parfenev, and M. A. Shakhov, *Sov. Phys. Solid State*, 612 (1986).

[59] S. Sasaki, Z. Ren, A. A. Taskin, K. Segawa, L. Fu, and Y. Ando, *Phys. Rev. Lett.* **109**, 217004 (2012).

[60] Y. Tanaka, Z. Ren, T. Sato, K. Nakayama, S. Souma, T. Takahashi, K. Segawa, and Y. Ando, *Nat Phys* **8**, 800 (2012).

[61] S.-Y. Xu, C. Liu, N. Alidoust, M. Neupane, D. Qian, I. Belopolski, J. Denlinger, Y. Wang, H. Lin, L. Wray, G. Landolt, B. Slomski, J. Dil, A. Marcinkova, E. Morosan, Q. Gibson, R. Sankar, F. Chou, R. Cava, A. Bansil, and M. Hasan, *Nat Phys* **8**, 800 (2012).

[62] T. Sato, Y. Tanaka, K. Nakayama, S. Souma, T. Takahashi, S. Sasaki, Z. Ren, A. A. Taskin, K. Segawa, and Y. Ando, *Phys. Rev. Lett.* **110**, 206804 (2013).

[63] A. C. Lent, M. S. Bowen, J. D. Dow, R. S. Alligaier, O. F. Sankey, and E. S. Ho, *Superlattices Microstruct* **2**, 491 (1986).

[64] M. Novak, S. Sasaki, M. Kriener, K. Segawa, and Y. Ando, *Phys. Rev. B* **88**, 140502 (2013).

[65] A. S. Erickson, J.-H. Chu, M. F. Toney, T. H. Geballe, and I. R. Fisher, *Phys. Rev. B* **79**, 024520 (2009).

[66] G. Balakrishnan, L. Bawden, S. Cavendish, and M. R. Lees, *Phys. Rev. B* **87**, 140507 (2013).

[67] M. Saghir, J. A. T. Barker, G. Balakrishnan, A. D. Hillier, and M. R. Lees, *Phys. Rev. B* **90**, 064508 (2014).

[68] L. P. He, Z. Zhang, J. Pan, X. C. Hong, S. Y. Zhou, and S. Y. Li, *Phys. Rev. B* **88**, 014523 (2013).

[69] M. Sigrist and K. Ueda, *Rev. Mod. Phys.* **63**, 239 (1991).

[70] K. Ueda and T. M. Rice, *Phys. Rev. B* **31**, 7114 (1985).

[71] E. I. Blount, *Phys. Rev. B* **32**, 2935 (1985).

[72] P. W. Anderson, *Phys. Rev. B* **30**, 4000 (1984).

[73] A. Umerski, *Phys. Rev. B* **55**, 5266 (1997).

[74] C.-K. Chiu, H. Yao, and S. Ryu, *Phys. Rev. B* **88**, 075142 (2013).

[75] K. Shiozaki and M. Sato, *Phys. Rev. B* **90**, 165114 (2014).

[76] T. Morimoto and A. Furusaki, *Phys. Rev. B* **88**, 125129 (2013).

[77] A. Altland and M. R. Zirnbauer, *Phys. Rev. B* **55**, 1142 (1997).

[78] A. Kitaev, *AIP Conference Proceedings* **1134** (2009).

[79] S. Ryu, A. P. Schnyder, A. Furusaki, and A. W. W. Ludwig, *New Journal of Physics* **12** (2010).

[80] A. P. Schnyder, S. Ryu, A. Furusaki, and A. W. W. Ludwig, *Phys. Rev. B* **78**, 195125 (2008).

[81] M. Sato, *Phys. Rev. B* **81**, 220504 (2010).

[82] T. Fukui, Y. Hatsugai, and H. Suzuki, *Journal of the Physical Society of Japan* **74**, 1674 (2005).

[83] Y. Ueno, A. Yamakage, Y. Tanaka, and M. Sato, *Phys. Rev. Lett.* **111**, 087002 (2013).

[84] H. Ozawa, A. Yamakage, M. Sato, and Y. Tanaka, *Phys. Rev. B* **90**, 045309 (2014).

[85] P. Goswami and B. Roy, *Phys. Rev. B* **90**, 041301 (2014).